Supplementary Figure 1

a. In vitro validation of probes

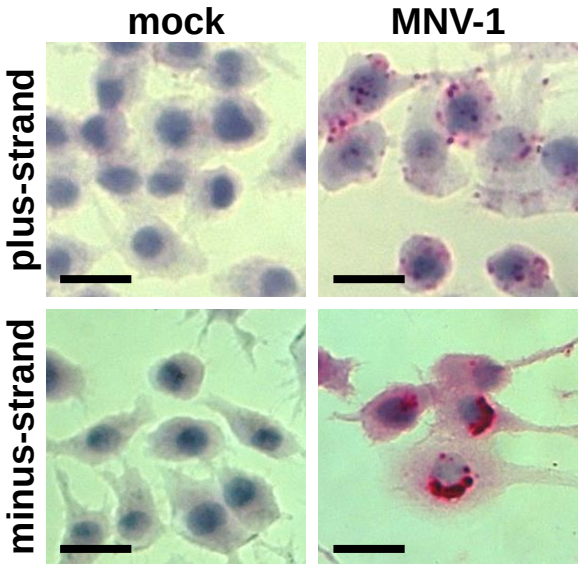

b. In vivo experimental approach

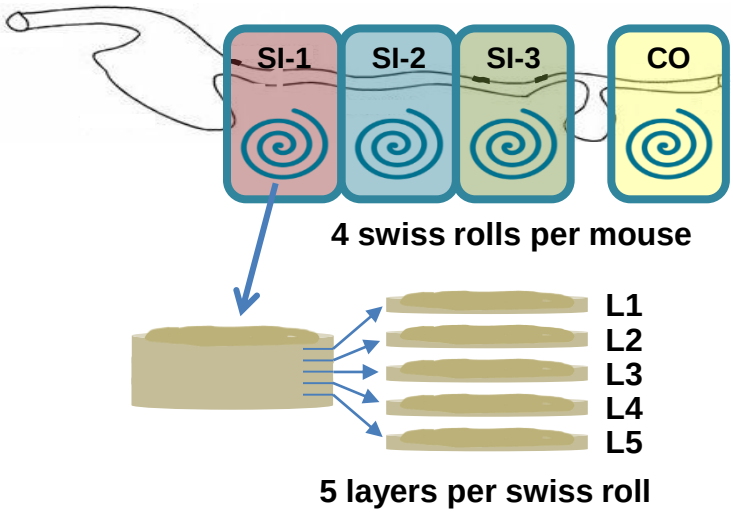

c. Control probes

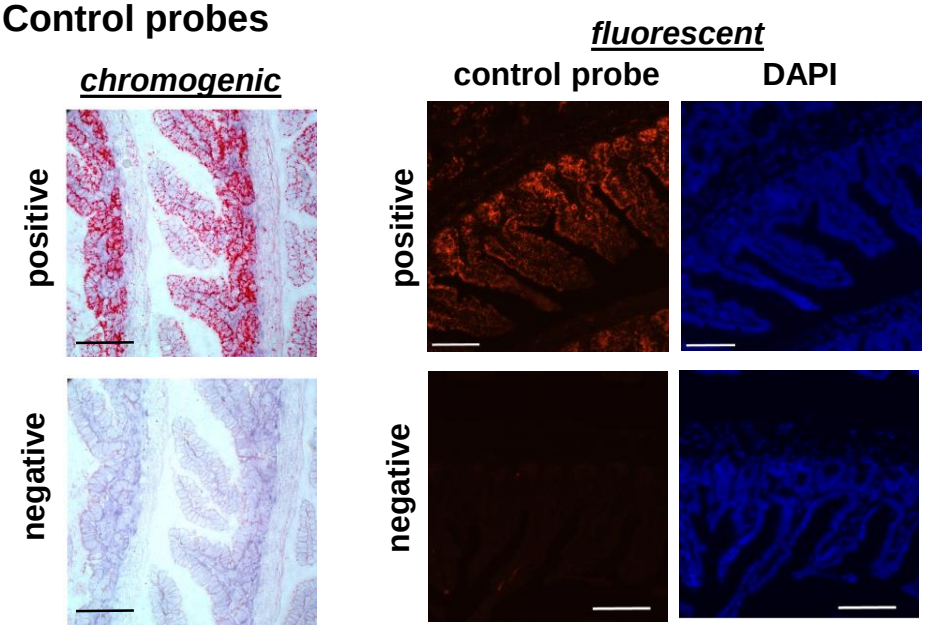

d. Naive intestinal sections hybridized with virus probes

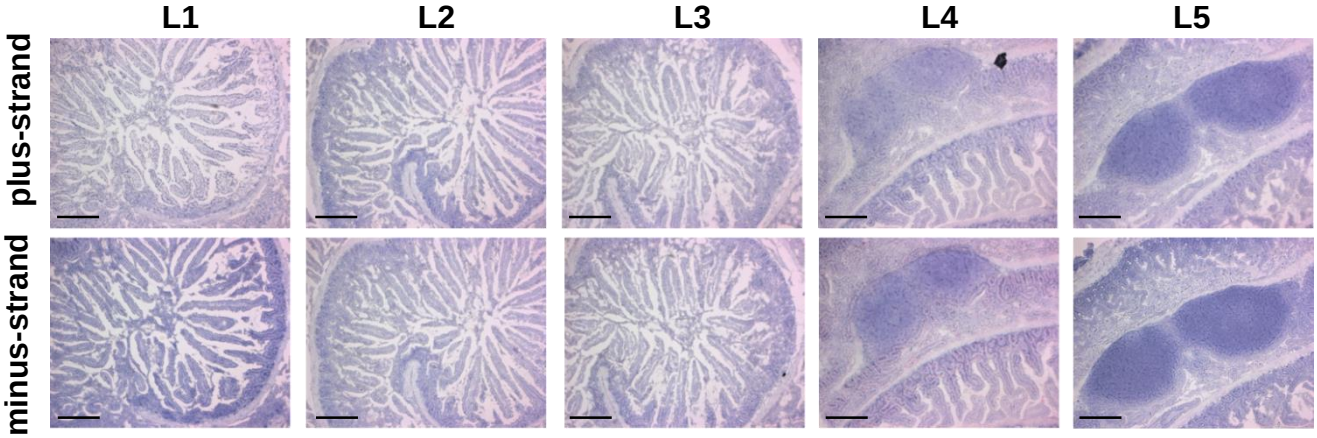

Supplementary Figure 1. Validation of RNAscope methodology to detect MNV-1-infected cells. a) Representative images of the murine Mϕ cell line RAW264.7 infected with mock inoculum or MNV-1 at MOI 5. Cells were hybridized with probes specific to either viral plus-strand genomic or minus-strand antigenomic RNA at 16hpi. This experiment was performed three times on duplicate samples, and representative images are shown. While plus-strand genomic RNA was detected throughout the cytoplasm of infected cells, minus-strand antigenomic RNA primarily localized to discrete perinuclear sites. This pattern is consistent with the accumulation of viral nonstructural proteins and double-stranded RNA in perinuclear replication factories[32]. Scale bars indicate 20µm. **b)** In order to exhaustively probe the mouse intestine for the presence of virus-infected cells, the entire small intestine (SI) was dissected into three equivalent lengths (referred to as SI-1, SI-2, and SI-3) and each segment was cut longitudinally, flattened, and rolled. The colon was processed as one segment (referred to as CO). Each swiss roll was fixed, paraffin-embedded, and processed for microscopic analysis by cutting serial sections from each of five sequential layers 500 µm apart. **c)** To confirm detection sensitivity and specificity as well as RNA integrity in the tissue sections, swiss rolls were hybridized with positive or negative control probes developed by ACDBio and detected using either chromogenic RNAscope ISH or RNAscope FISH assays. The PPIB cellular housekeeping gene transcript was used as the positive control probe target, while the dapB bacterial gene transcript was used as the negative control probe target. Scale bars indicate 100µm. **d)** Serial sections from each of the five layers of SI-3 of a representative naive mouse were incubated with RNAscope probes designed to hybridize with either the plus-strand MNV-1 genomic RNA (top panels) or the minus-strand replication intermediate (bottom panels). Scale bars indicate 200µm. The vertical lines apparent in certain images are a byproduct of the image stitching process used by the slide scanner to create high-resolution images (see Methods).

Supplementary Figure 2

a. MNV-1 tissue titers

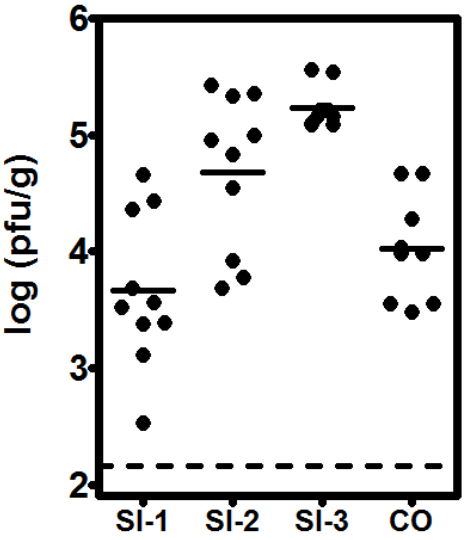

b. Intestinal sections hybridized with MNV-1 plus-strand probe

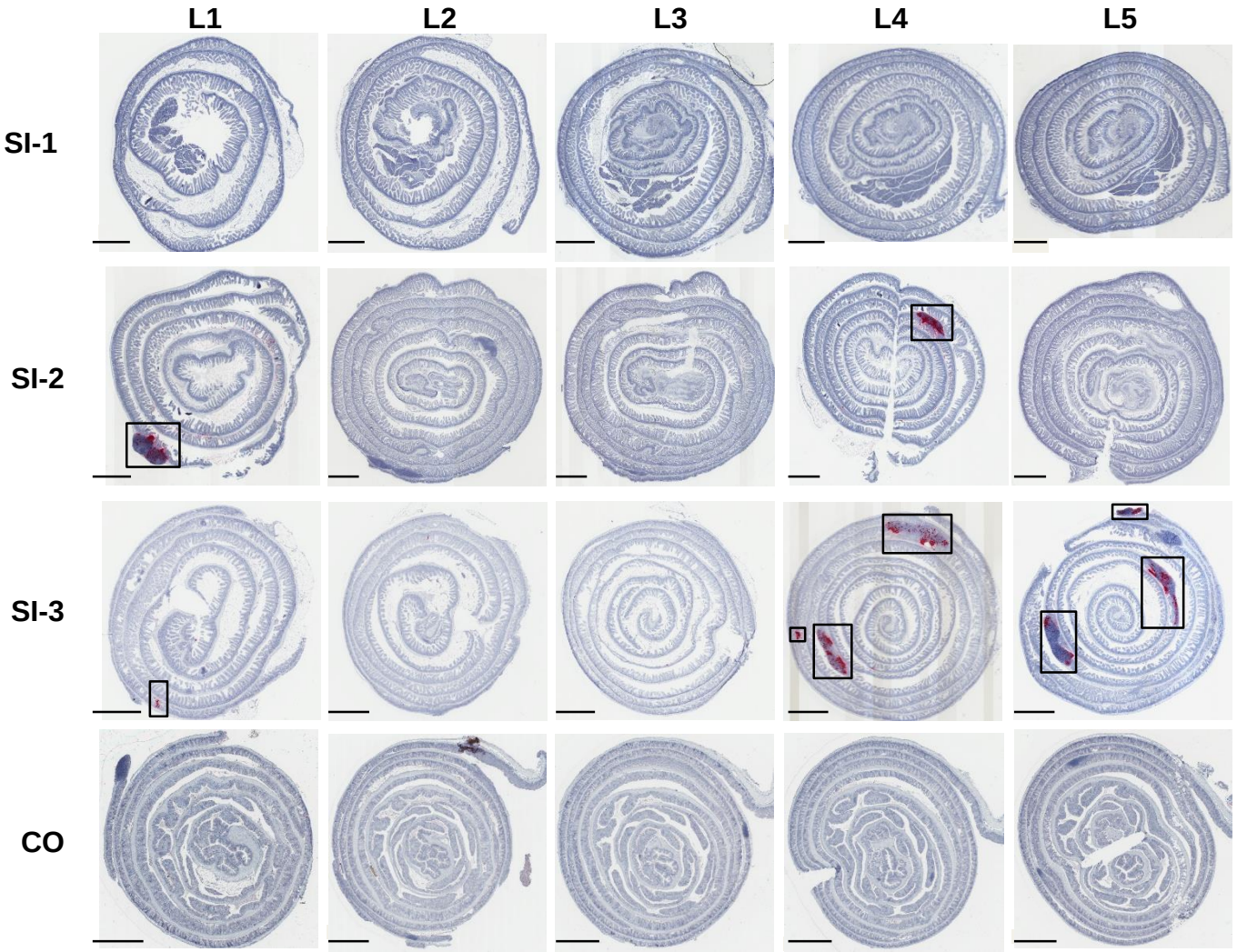

c. Intestinal sections hybridized with MNV-1 minus-strand probe

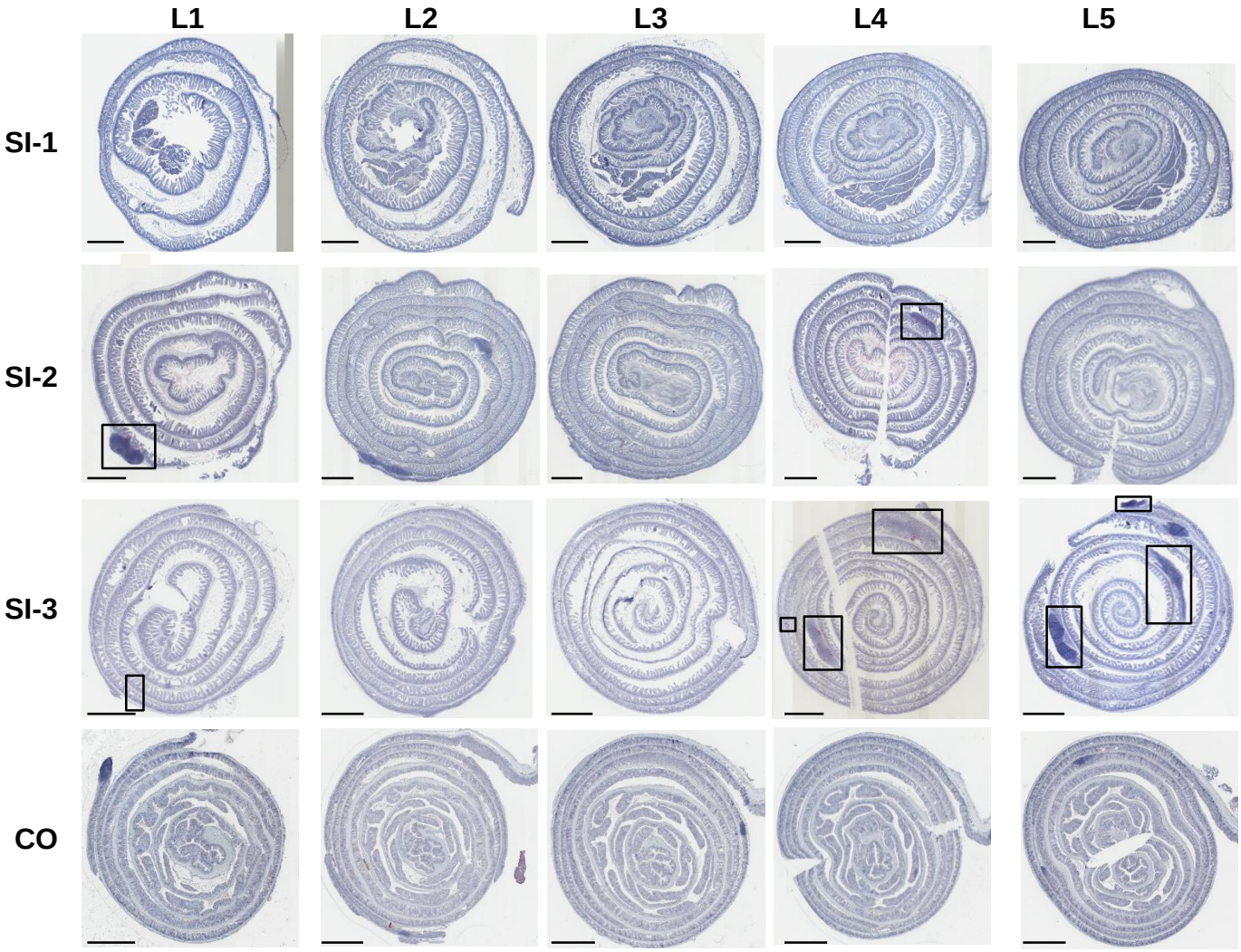

Supplementary Figure 2. MNV-1 infects the GALT within the distal two-thirds of the small intestine. a) Groups of B6 mice (*n* = 5) were infected p.o. with 10^7 $TCID_{50}$ units MNV-1 and the segments of the intestine indicated on the *x*-axis were dissected at 24 hpi. Virus titers were determined by standard plaque assay. The entire experiment was repeated twice, and all titers are displayed in the graph. **b-c)** Sections from each of the five layers of each intestinal segment of MNV-1-infected mice at 24 hpi were incubated with RNAscope probes designed to hybridize with the plus-strand genomic RNA **(b)** or the minus-strand anti-genomic RNA **(c)** of MNV-1. The boxed areas within the tissue section represent viral foci of infection. Scale bars represent 1mm. The vertical lines apparent in certain images are a byproduct of the image stitching process used by the slide scanner to create high-resolution images (see Methods).

Supplementary Figure 3

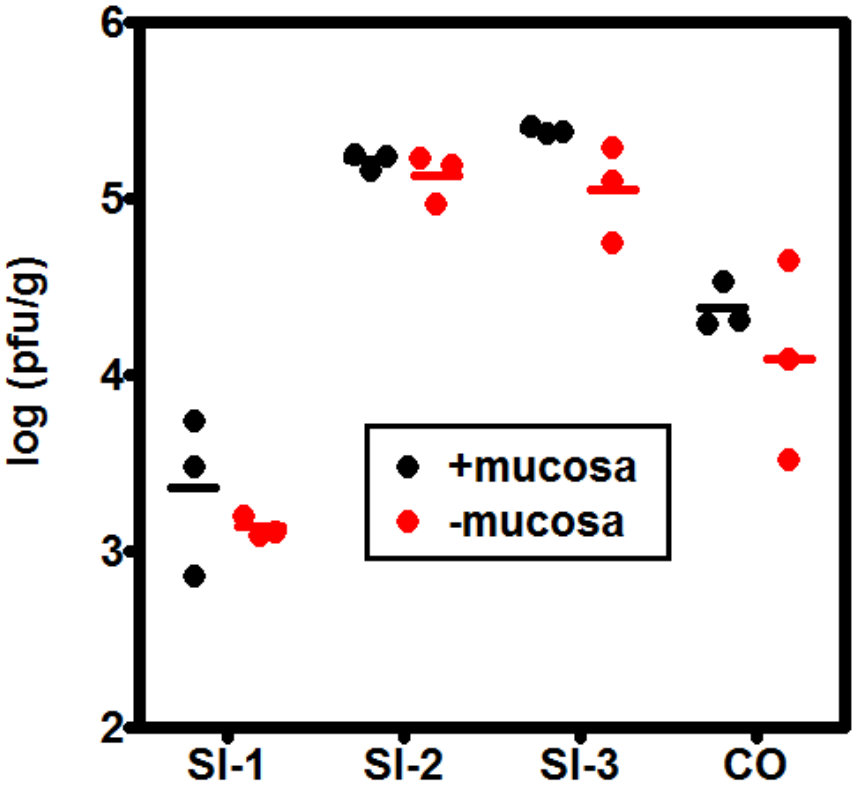

Supplementary Figure 3. Virus titers are not reduced by removal of the intestinal mucosa. The indicated segments of the GI tract were dissected from groups of B6 mice (*n* = 3) infected with 10^6 TCID50 units MNV-1 p.o. for 24 h using our standard method of removing the intact tissue piece (+mucosa, black dots); or using a modified technique whereby the intestinal pieces were cut open longitudinally, scraped with a plastic cell spreader to remove the mucus layer, and rinsed vigorously for 15 s with 15 ml PBS three times (-mucosa, red dots). Tissue pieces were homogenized and infectious virus titered by plaque assay.

Supplementary Figure 4

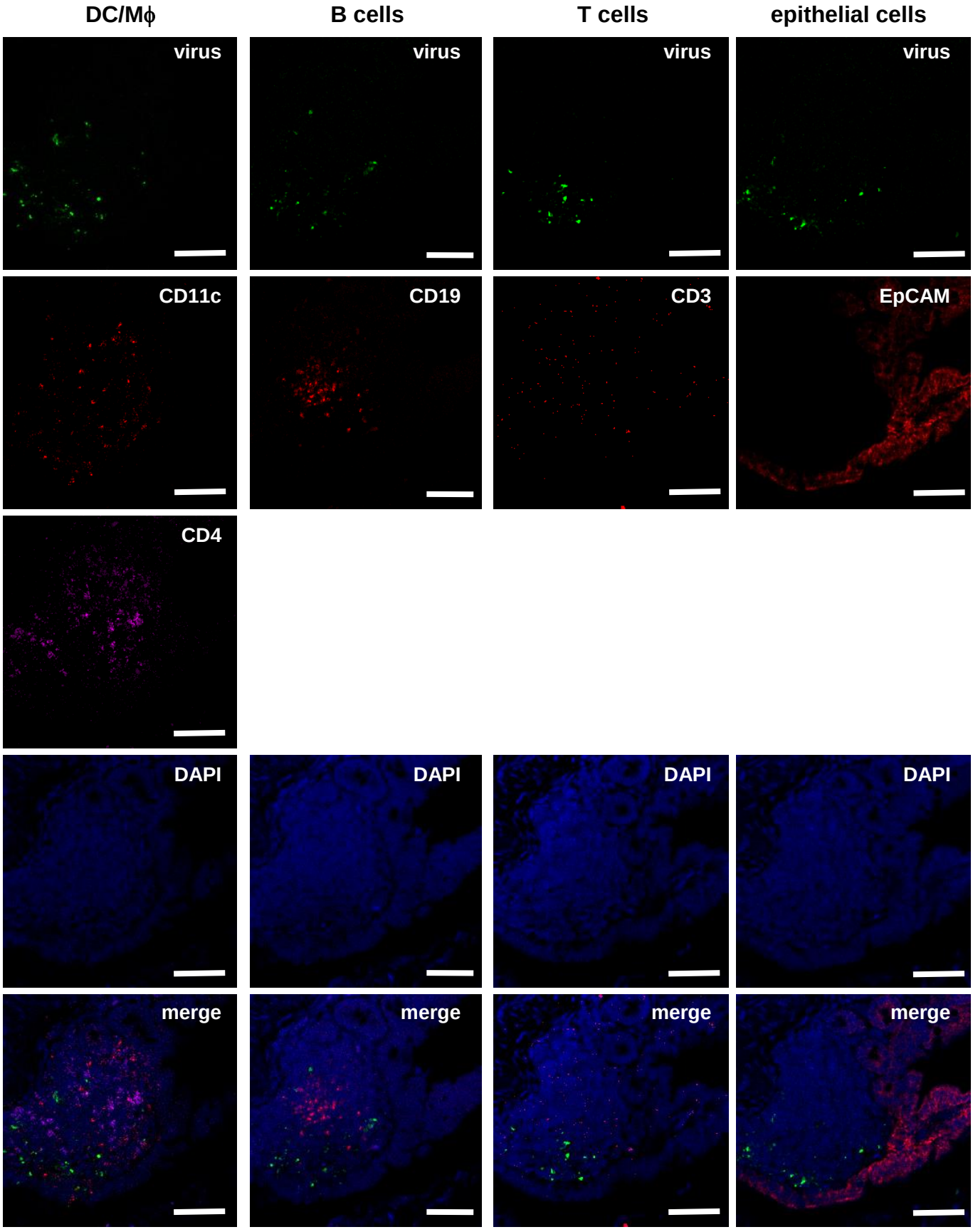

Supplementary Figure 4. The expected GALT cellular distribution is detected using cell-specific RNAscope probes, and viral replication occurs predominantly in the SED. Individual fluorescence channels corresponding to the merged images presented in Fig. 2A are presented here for clarity. The merged images are included as well. Scale bars indicate 50µm.

Supplementary Figure 5

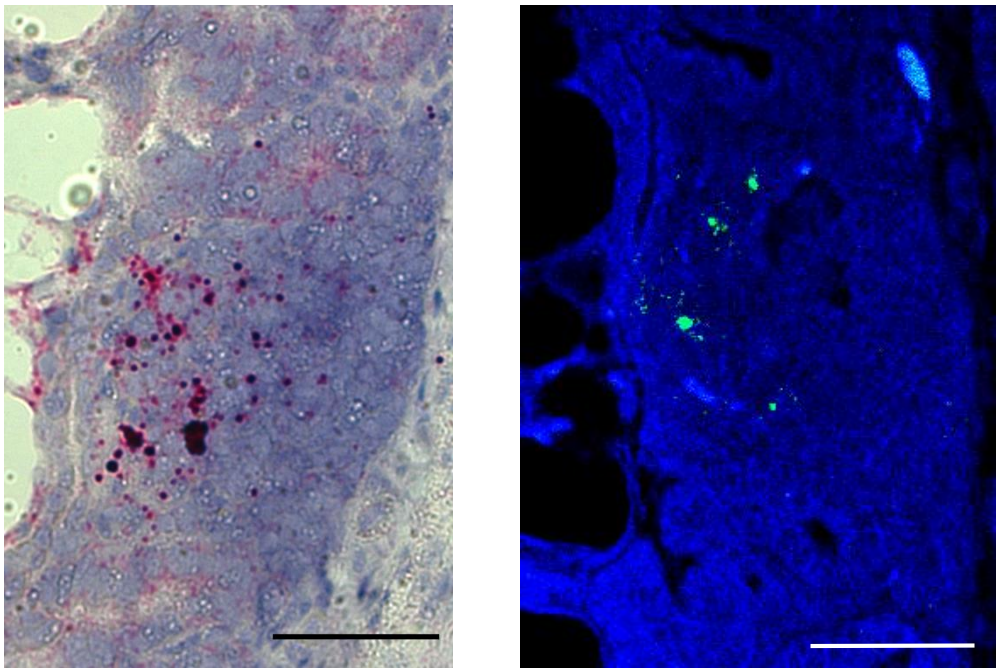

Supplementary Figure 5. Sensitivity difference in chromogenic and fluorescent RNAscope assays to detect viral minus-strand genomes. Serial sections of SI-3 from a representative MNV-1-infected B6 mouse at 24 hpi were hybridized with the MNV-1 minus-strand viral RNA-specific probe and visualized using chromogenic ISH (left; shown in red) or FISH (right; shown in green). This difference in sensitivity was observed in every instance where chromogenic and fluorescent assays were performed on serial sections from the same tissue piece. Scale bars represent 50µm.

Supplementary Figure 6

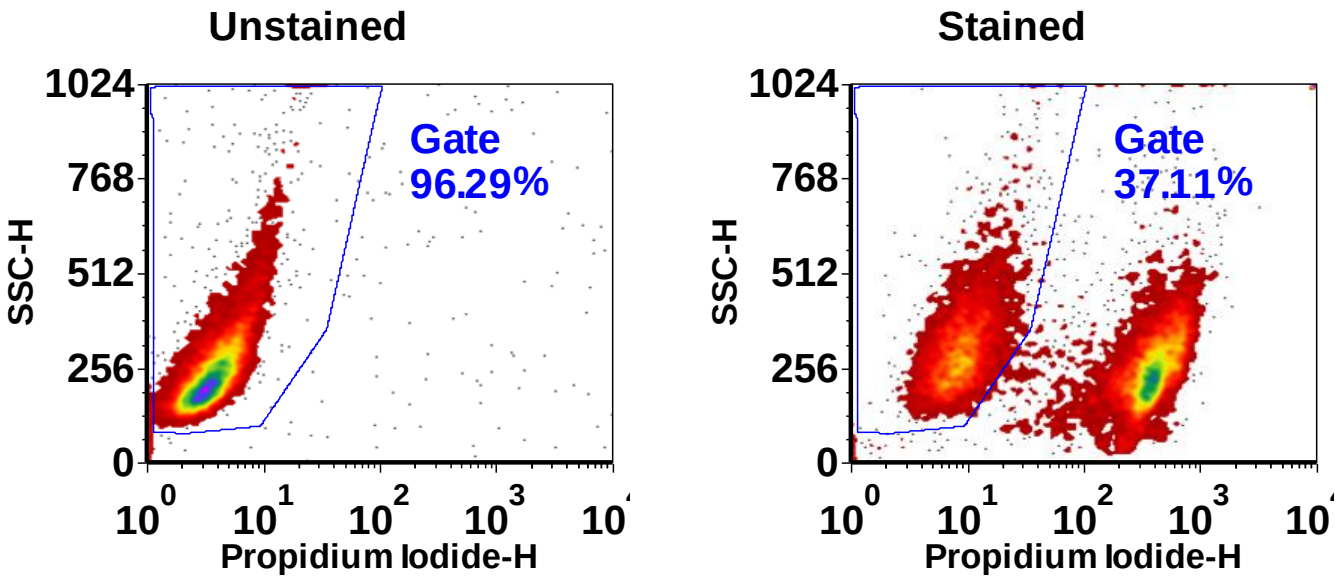

Supplementary Figure 6. Representative gating strategy for propidium iodide staining. To quantify cell viability, cell lines were stained with propidium iodide (PI) before data acquisition using a BD FACS Calibur and BD CellQuest Pro software. Unstained cells were used to set a gate for viable PI-negative cells.

Supplementary Figure 7

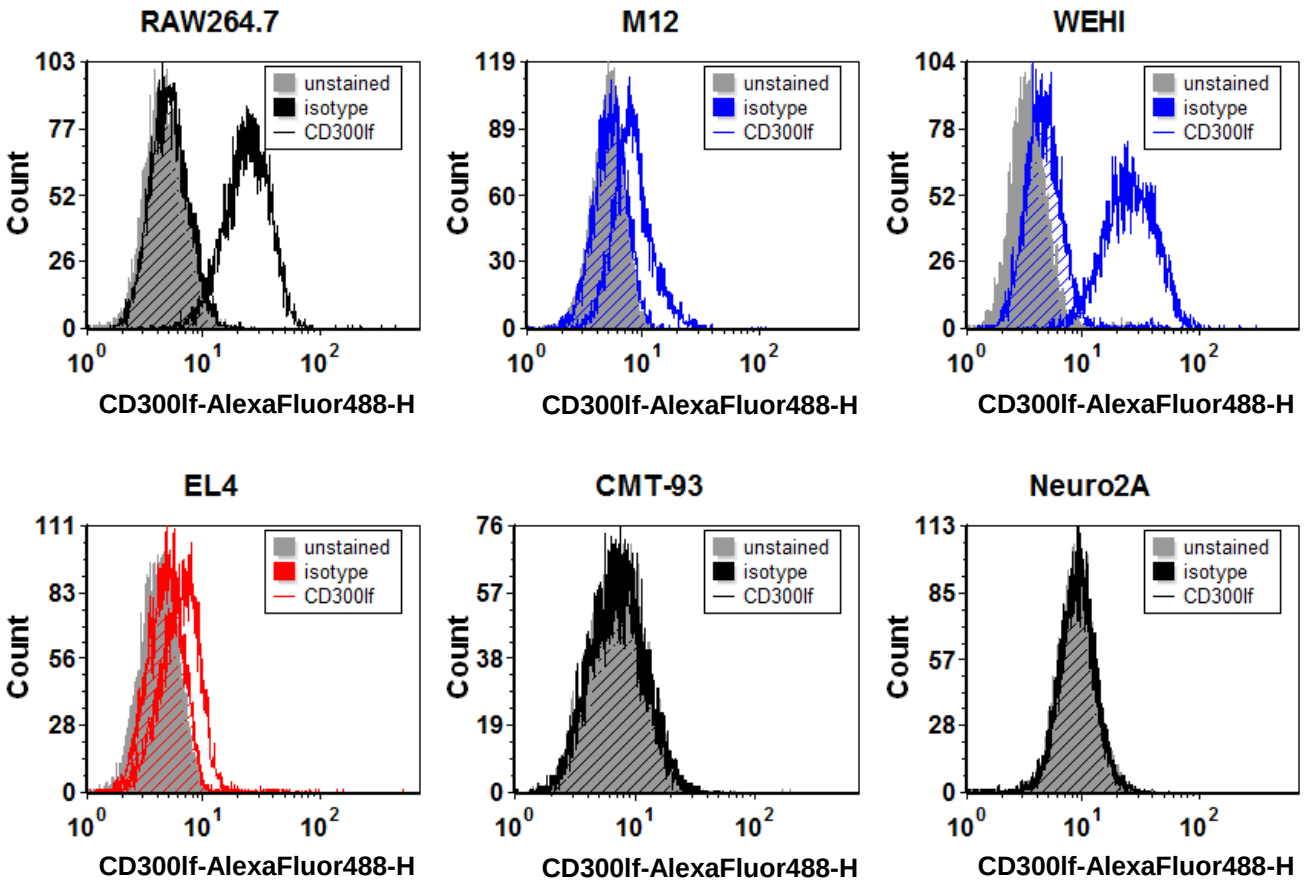

Supplementary Figure 7. Representative flow cytometric data used to determine frequency and abundance of CD300lf on cell lines. The indicated cell lines were either unstained (gray filled peaks), stained with an isotype control antibody (hatched peaks), or stained with an anti-CD300lf antibody (solid lines). Markers were set using the isotype control stained sample. Duplicate samples stained with isotype and CD300lf antibodies were tested for each condition, and the entire experiment repeated three times.

Supplementary Figure 8

a. General gating strategy

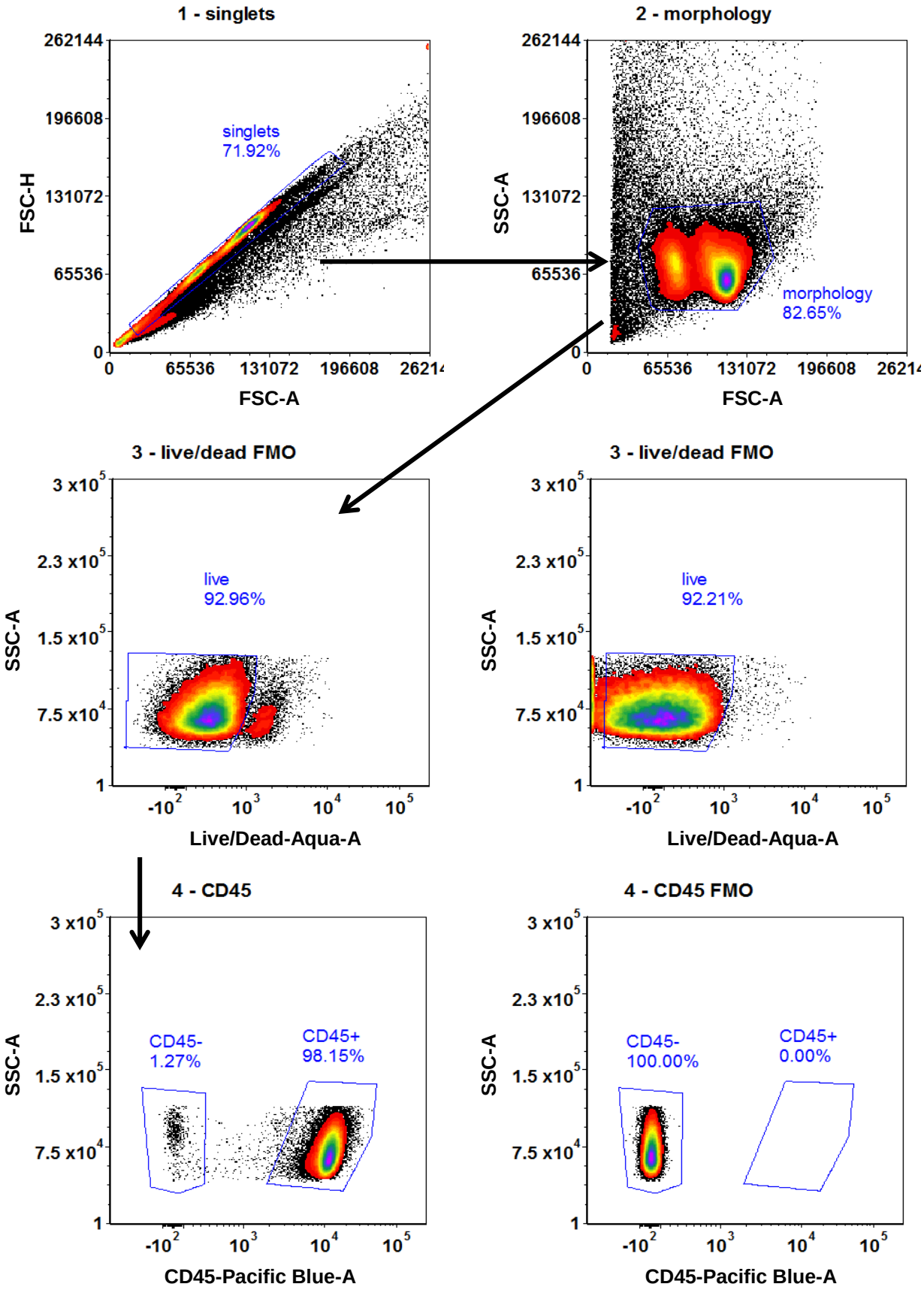

b. Gating strategy for defining cell types

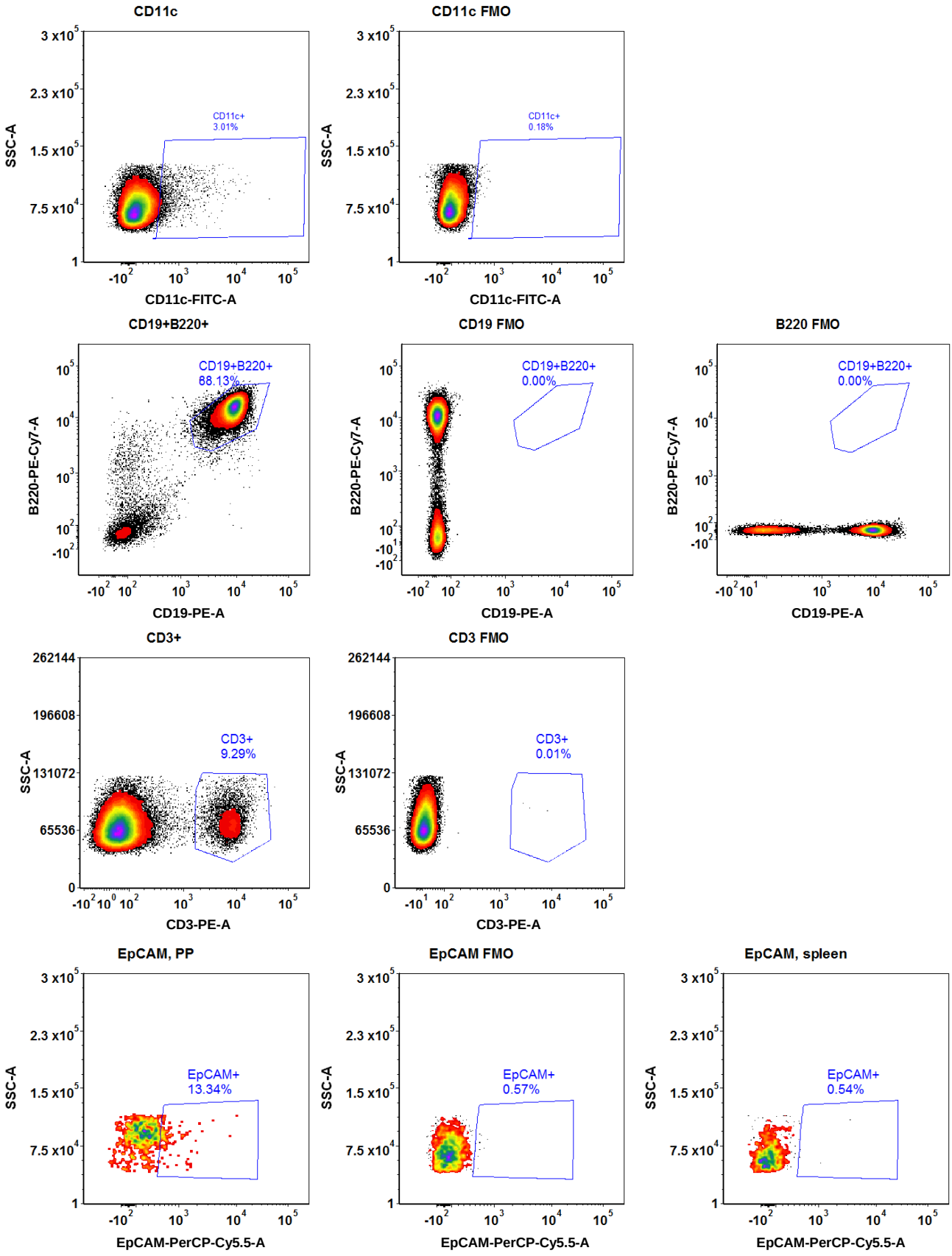

c. CD300lf analysis on defined cell types

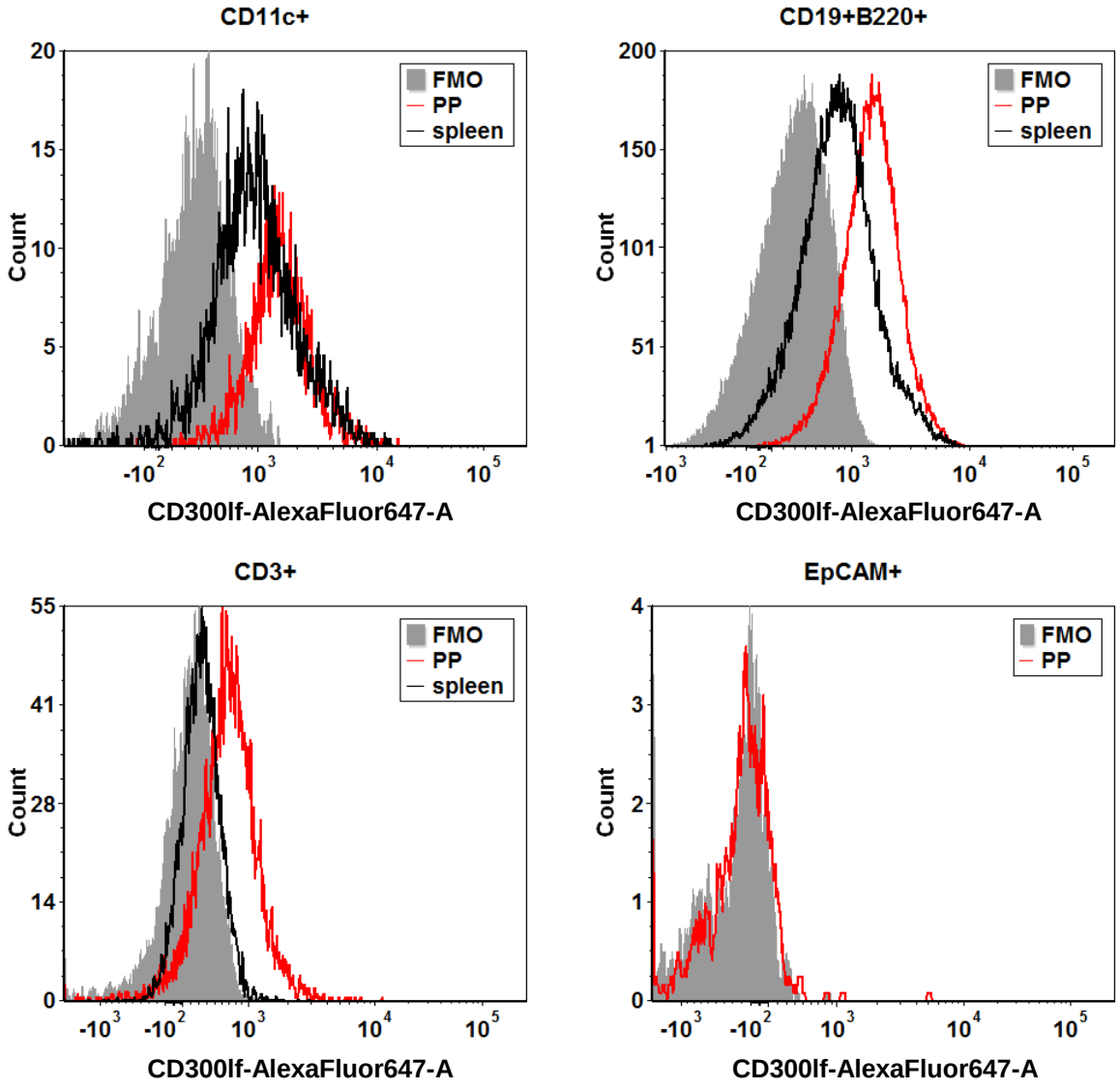

Supplementary Figure 8. Representative flow cytometric data used to determine frequency and abundance of CD300lf on Peyer's patch cells. CD300lf expression was quantified on Peyer's patch cells from naïve B6 mice. Multicolor flow cytometry data were acquired using a BD LSR-II and FACS Diva software. **a)** After doublet exclusion, cells were gated based on morphology, live/dead stain, and CD45 expression. **b)** In antibody panel 1, $CD45^+$ cells were further defined DC/Mϕ ($CD11c^+$) or B cells ($CD19^+B220^+$). In antibody panel 2, $CD45^+$ cells that were $CD3^+$ were defined as T cells and $CD45^-$ cells that were $EpCAM^+$ were defined as epithelial cells. As expected, a small frequency of $EpCAM^+$ cell was detected in Peyer's patch cell suspensions but not splenocytes. **c)** The frequency of $CD300lf^+$ cells in each population was determined based on CD300lf FMO control staining within each cell-type specific gate such that background within the $CD300lf^+$ gate did not exceed 1%.